



# Predictive model of yaw error in a wind turbine



Tinghui Ouyang, Andrew Kusiak\*, Yusen He

Department of Mechanical and Industrial Engineering, 3131 Seamans Center, The University of Iowa, Iowa City, IA 52242, USA

## ARTICLE INFO

### Article history:

Received 26 September 2016

Received in revised form

18 December 2016

Accepted 30 January 2017

Available online 31 January 2017

### Keywords:

Wind direction prediction

Yaw control

Data mining

Data transformation

Time series

## ABSTRACT

The yaw position of a wind turbine is adjusted in response to the changing wind direction for maximum energy extraction. A data-mining approach is proposed to predict wind direction. To accommodate the full range of yaw motion, the wind direction data is transformed into two time series (sine value and cosine values). Parameters of the time series are selected for predictive modeling. Four data-mining algorithms are applied to build prediction models. Industrial data is used to develop, validate, and test the proposed models. Computational experience with data representing four seasons and four sampling frequencies is reported in this paper.

© 2017 Elsevier Ltd. All rights reserved.

## 1. Introduction

Growing awareness of global warming has led to interest in renewable energy. Wind and photovoltaic generation have experienced the fastest growth in the past two decades [1]. The world's combined wind generation will provide 11.5%–12.3% of electricity by 2020 [2]. To realize this goal, improvement in wind energy technology and performance of the deployed assets is needed.

Predictive technologies are key to performance of wind generators due to variability of the wind. It is a common practice to shut off wind turbines due to high and variable speed wind [3]. Some generation losses are encountered due to misalignment between the rotor and wind direction. Prediction of wind speed and wind direction are important for wind generation.

A wind speed prediction system shuts off a turbine when wind speed becomes too large. A power prediction system impacts stability of the electric power system. The prediction approaches discussed in the literature fall into two categories [4], with the physics-based models making the first category. Models have been proposed to predict wind speed by fusing terrain, temperature, pressure, and data from numerical weather prediction systems (NWPs) [5]. The predicted wind speed constitutes a basis for power prediction. The second category encompasses models versed in statistics. Models such as auto-regression and moving average

(ARMA) use either wind speed or the wind power time series as the input [6]. Three neural networks (NNs) were proposed to predict wind speed in Ref. [7]. Algorithms such as fuzzy logic methods, support vector machine models, Kalman filters, and hybrid methods, have been applied to predict wind speed or wind power [8–10].

Besides the wind speed, wind direction is a significant factor impacting the energy output [11]. Since wind direction is an angular variable, as opposed to the scalar variables such as wind speed, temperature, and wind power, it offers limitations in direct use in prediction models. In most published literature, wind direction is predicted along with wind speed. Yang et al. [12] applied Bayesian approach to build models predicting wind speed, wind direction, and ambient temperature. In Ref. [13], a circular regression model was developed to predict wind direction by applying bias correction and ensemble calibration techniques. Wind direction was used to decompose wind speed into lateral and longitudinal components, wind direction was computed based on predicted values of these two components in Ref. [14]. In some cases, wind direction was predicted by wind vector, for example, historical “similar days” were used to predict wind vector in Ref. [15]. An adaptive neuro-fuzzy inference system was developed in Ref. [16]. Wind direction was also predicted in other applications, including pollution management and ship routing. For example, a model predicting wind direction was developed to track volcanic ash in Ref. [17]. The predicted wind direction was applied to forecast the ozone and pollutant levels in Refs. [18,19].

In the published literature on prediction of wind direction, two

\* Corresponding author.

E-mail address: [andrew-kusiak@uiowa.edu](mailto:andrew-kusiak@uiowa.edu) (A. Kusiak).

issues stand out. The first one is that wind direction is an angular variable with a period of  $360^\circ$ . The latter implies that general prediction algorithms applied to a periodic variable, e.g., wind direction, do not work well. Therefore, transforming the wind direction into a linear form is the first step. Lateral and longitudinal wind speed were applied to express wind direction in Ref. [20]. A link function was proposed in Ref. [21] to transform wind direction into a linear variable. The second issue is that of prediction accuracy of wind direction which impacts energy generation.

A new model predicting wind direction is proposed in this paper (shown in Fig. 1). Trigonometric functions and data mining algorithms were adopted to predict wind direction. The sine and cosine functions transform wind direction into a linear variable. The range of wind direction  $[0^\circ, 360^\circ]$  is mapped into  $[-1, 1]$ . The prediction model developed in this paper was developed with data mining algorithms. This approach is suitable for capturing dynamic phenomena hidden in big data.

The paper is organized in six sections. Section 2 analyzes the properties of the selected wind data sets. The proposed method is described in Section 3. Details of transformation of the wind direction data are also included. Section 4 offers modeling details of wind direction prediction. Section 5 discusses the prediction results. Section 6 concludes the paper.

## 2. Data source and analysis

The wind data used in this paper to predict wind direction was obtained from an operating wind farm. The data was collected in the period June 1st, 2014 to July 1st, 2015 at 10 min intervals. The total number of data points is 57024.

A brief analysis of the historical data indicates that wind direction has obvious seasonal features affecting the yaw of wind turbines. Fig. 2 shows rose diagrams of wind direction over four seasons of a year.

Fig. 2(a) shows the wind direction data in the summer season (June, July and August) with the prevailing direction around  $180^\circ$ . Similarly, Fig. 2(b)–(d) are for the fall (September, October, and November), winter (December, January, and February), and spring (March, April, and May), respectively. The prevailing wind direction in Fig. 2(c) is about  $315^\circ$ . There are more than two prevailing directions around  $180^\circ$  and  $315^\circ$  in the fall and spring.

Fig. 3 illustrates the rose diagram of wind direction over a year period. Two wind directions around  $180^\circ$  and  $315^\circ$  are prevailing. It is concluded from Figs. 2 and 3 that wind in the analyzed data set has seasonal features. Wind turbines are usually yawed around the prevailing directions.

Fig. 4 depicts the mean wind speed of four seasons. Wind is stronger in the fall and winter than in the spring and summer. This implies that most energy is generated in the second half of a year. Prediction of wind direction is more important in the strong wind seasons.

## 3. Data transformation

Prediction of wind direction is important to yaw control. When wind direction changes, the rotor of a wind turbine is aligned to face the wind direction. Any misaligned (yaw error) results in

production losses. Based on the predicted wind direction, the nacelle is adjusted to reduce the yaw error.

Historical wind direction data is crucial to predict wind direction. Fig. 5 shows the variability of wind direction in time. It can be observed that the wind direction is not a continuous and linear variable, e.g., area A in Fig. 5.

In Ref. [20], the wind velocity vector was decomposed into lateral and longitudinal components in (1), which containing the information of wind direction.

$$\begin{cases} v_x = v \sin(\theta - \bar{\theta}) \\ v_y = v \cos(\theta - \bar{\theta}) \end{cases} \quad (1)$$

where:  $v_x$  and  $v_y$  are the lateral and longitudinal components of the wind speed, respectively;  $\theta$  is the direction of wind vector; and  $\bar{\theta}$  is the mean direction. The predicted direction is determined from the predicted  $v_x$  and  $v_y$ . The link function (2)–(3) was proposed in Ref. [21] to transform the circular variable into a linear variable.

$$g(u) = 2\pi \left( \Phi(u) - \frac{1}{2} \right) + \mu \quad (2)$$

$$g^{-1}(x) = \Phi^{-1} \left( (x - \mu) / 2\pi + \frac{1}{2} \right) \quad (3)$$

where:  $\Phi(u)$  is the standardized Gaussian distribution function  $N(0,1)$ ;  $\mu$  is the mean direction in radians. Equation (3) is the inverse link function transforming the circular variable. Component models are more appropriate to predict wind direction. They predict wind direction using wind speed, and thus the direction prediction accuracy is affected by the wind speed. The approach proposed in this paper, the wind direction is directly predicted. As shown in Fig. 5, wind direction ranges from  $0^\circ$  to  $360^\circ$ . Assuming wind direction  $\theta$ , the sine and cosine functions of  $\theta$  have positive or negative values in different quadrants, for example,  $(+, -)$  means the angle in the second quadrant having a positive sine value and negative cosine value (see Fig. 6).

The equations for transforming wind direction are defined in (4).

$$\begin{cases} y_1 = \sin(\theta) \\ y_2 = \cos(\theta) \end{cases} \quad (4)$$

where:  $\theta$  represents the wind direction;  $y_1$  and  $y_2$  are the values of sine and cosine function, respectively. Fig. 7 shows the values of these two functions at the same period as in Fig. 5.

Based on the plot in Fig. 7, the sine and cosine functions do not include regions with rapidly changing value areas such as area A in Fig. 5. It is also obvious that the values of the two functions map into the four quadrants. Therefore, this transformation approach is adopted in building the prediction model of wind direction. The overall steps of prediction of wind direction is presented in Fig. 8.

The proposed approach follows the following steps:

Step 1: Pre-process the data from a wind farm, including the wind direction data.

Step 2: Apply the sine and cosine functions (4) to transform the

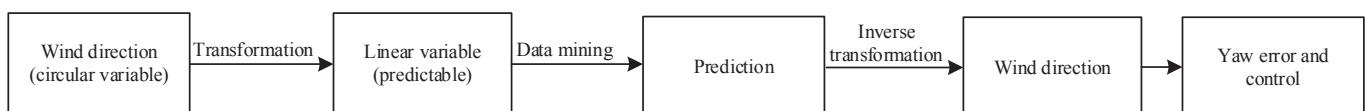


Fig. 1. Description of the proposed approach.

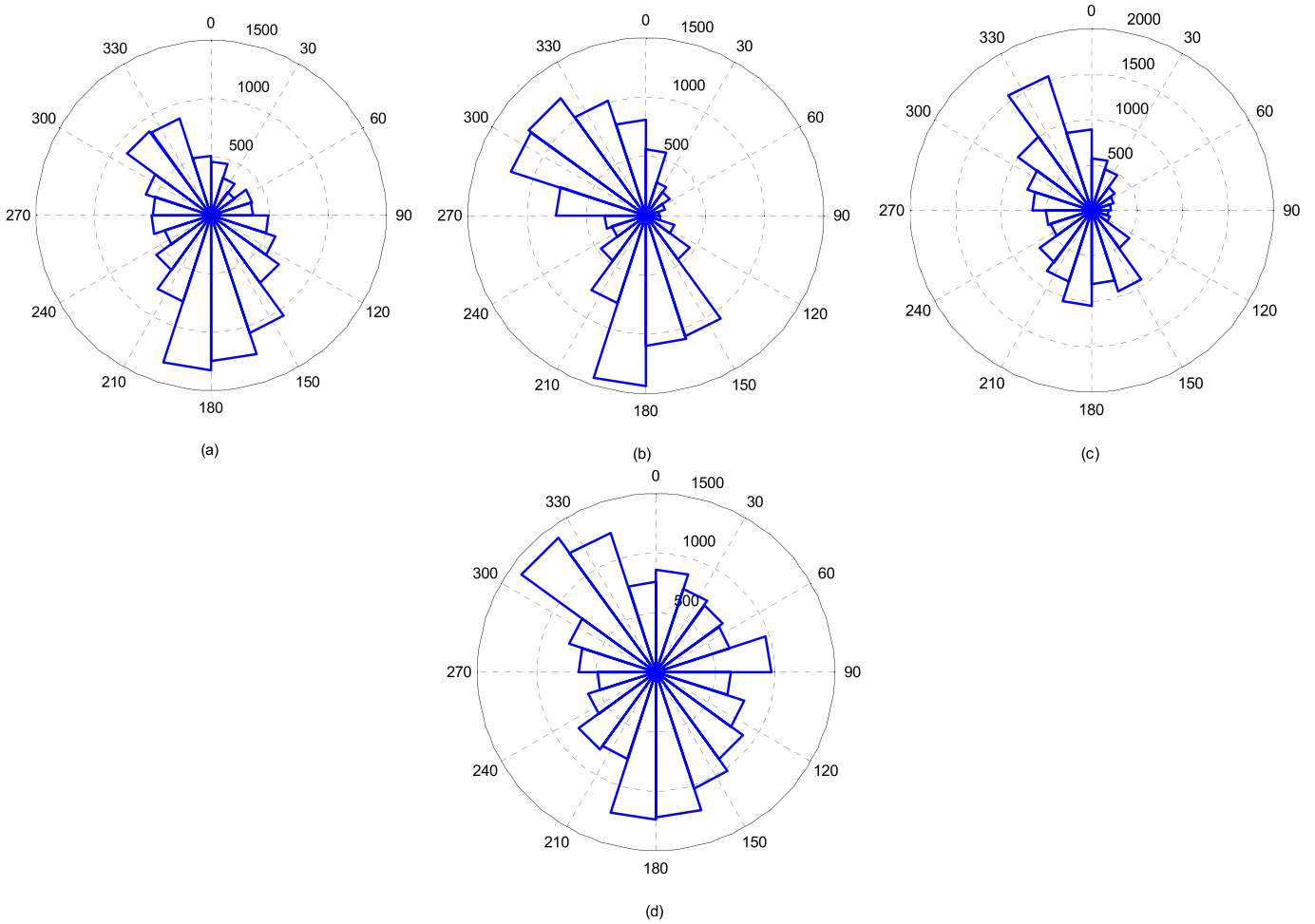


Fig. 2. Rose diagrams of wind direction over four seasons: (a) Summer; (b) Fall; (c) Winter; (d) Spring.

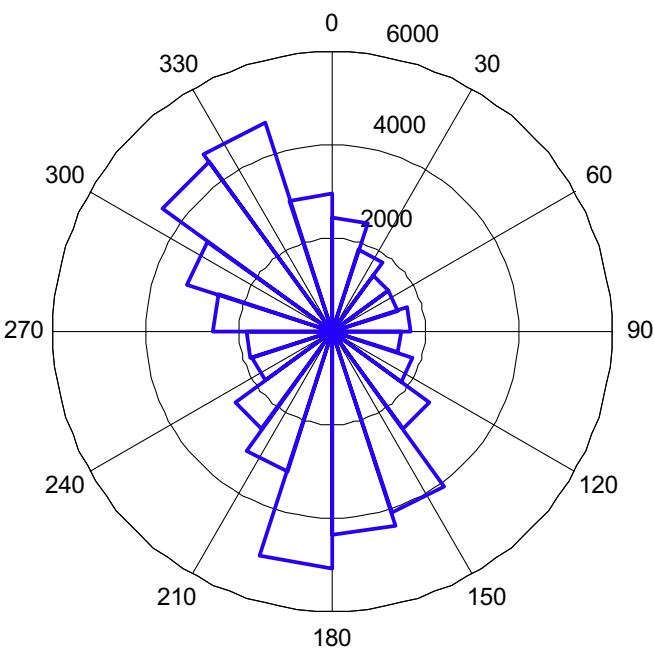


Fig. 3. Rose diagram of wind direction in the entire year.

wind direction data of Step 1.

Step 3: Select important parameters and data mining algorithms and build prediction models.

Step 4: Predict wind direction. Predict sine and cosine values, then use inverse trigonometric function to transform the predicted value into an angle.

Step 5: Apply the predicted angle to position the yaw of a wind turbine.

#### 4. Models for prediction of wind direction

##### 4.1. Basic models of sine and cosine values

The wind direction data is a time series, therefore the transformed sine and cosine values are also a time series. According to [6], historical data of time series play important roles in prediction of wind speed and direction. Based on [22], the past values of a parameter are employed in a time-series prediction model expressed in (5).

$$\hat{y}(t) = f(y(t - T), y(t - 2T), \dots, y(t - nT)) \tag{5}$$

where:  $\hat{y}(t)$  is the predicted value;  $y(t-nT)$  is the  $n$ th historical observed value; and  $T$  is the sampling interval. Assuming the transformed sine and cosine values of historical wind direction are  $s(t)$  and  $c(t)$ , the sampling interval  $T$  is 10 min, the prediction models of these two time series are defined as  $f$  and  $g$ , respectively.

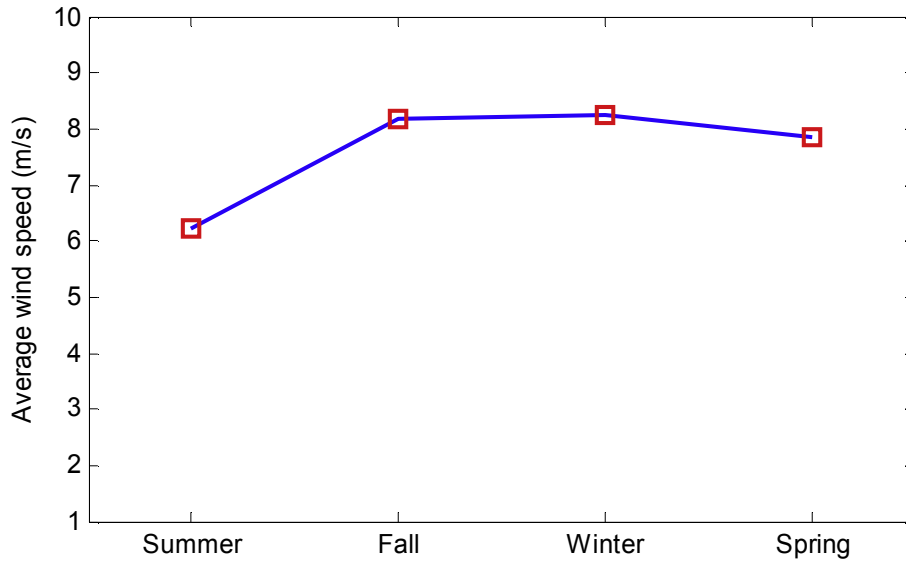


Fig. 4. Average wind speed over four seasons.

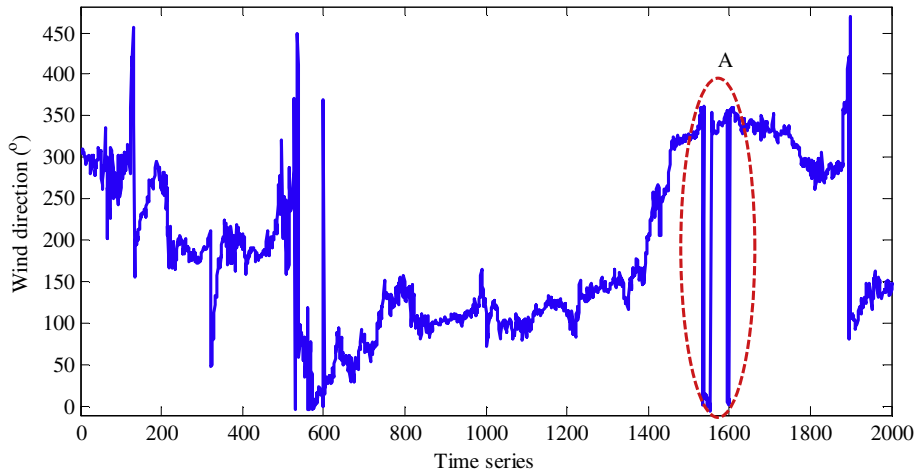


Fig. 5. Variability of wind direction time series.

The predicted values of  $s(t)$  and  $c(t)$  are related to the historical values of the sine function  $s(t)$ , cosine function  $c(t)$ , and the wind speed  $w(t)$ . The prediction models are defined in (6) and (7).

of a prediction model. The models (6)–(7) include  $p + q + r$  predictors. Algorithms such as the Boosted Trees Algorithm (BTA), Neural Network (NN), and Random Forest Algorithm (RFA) are used

$$s(t) = f(s(t - 1), s(t - 2), \dots, s(t - p), c(t - 1), c(t - 2), \dots, c(t - q), w(t - 1), w(t - 2), \dots, w(t - r)) \tag{6}$$

$$c(t) = g(s(t - 1), s(t - 2), \dots, s(t - p), c(t - 1), c(t - 2), \dots, c(t - q), w(t - 1), w(t - 2), \dots, w(t - r)) \tag{7}$$

where:  $w(t)$  represents the wind speed at time  $t$ ;  $p, q, r$  are the number of historical sine, cosine, and wind speed values, respectively. To limit the number of parameters, the initial dimension of each parameter in (6)–(7) has been based on the previous data analysis experience, e.g. the values of  $p, q,$  and  $r$  set at 5 here.

4.2. Parameter selection

Parameter selection is important for performance and accuracy

to select important parameters. In this paper, BTA is applied to determine the importance of parameters in models (6)–(7). The importance results are presented in Table 1.

The parameter rank in Table 1 is computed by setting the value of the most important parameter to 100. Then the importance of parameters is decided by normalizing the rank value.

Fig. 9 shows the plots of parameter importance used in models (6) and (7), respectively. It is obvious that  $s(t-1), \dots, s(t-5)$  are the most important parameters in predicting  $s(t)$ , and that  $c(t-1), \dots, c(t-$

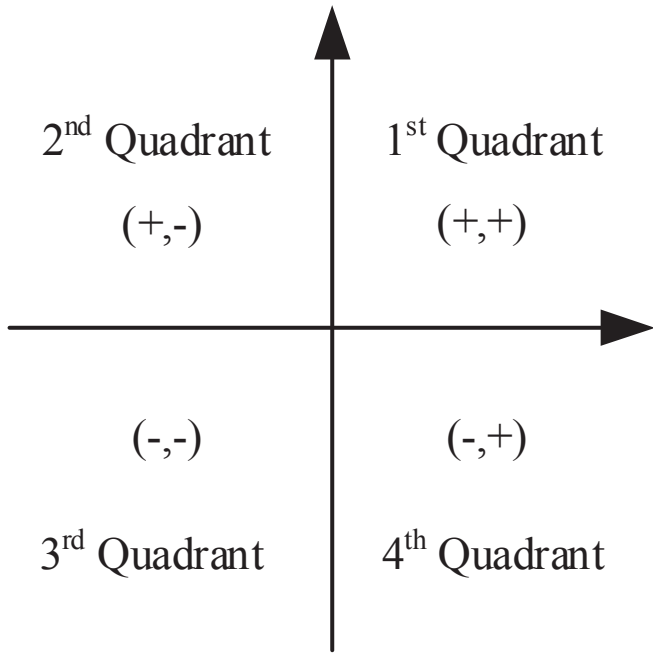


Fig. 6. Representation of sine and cosine functions in four quadrants.

5) are the most important parameters in predicting  $c(t)$ . To reduce dimension of the input, eight parameters according to Table 1 and Fig. 9 are selected out of 15. The prediction models (6)–(7) are expressed as (8)–(9).

$$s(t) = f(s(t - 1), s(t - 2), \dots, s(t - 5), c(t - 1), c(t - 2), c(t - 3)) \tag{8}$$

$$c(t) = g(c(t - 1), c(t - 2), \dots, c(t - 5), s(t - 1), s(t - 3), s(t - 2)) \tag{9}$$

### 4.3. Data mining algorithms

The prediction models studied in this paper are developed with data mining algorithms. Four algorithms, support vector machine

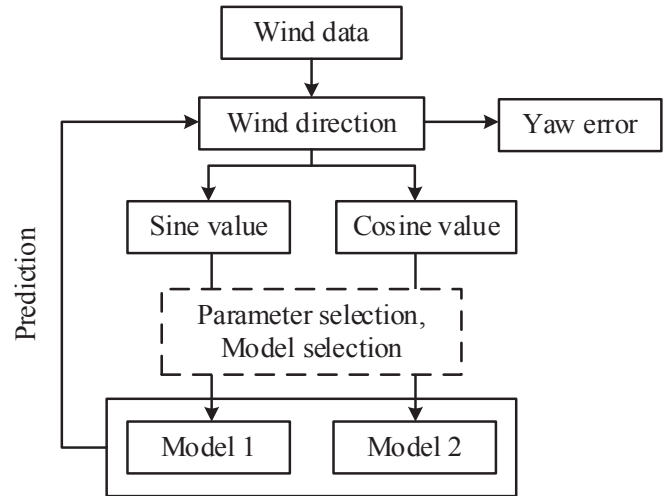


Fig. 8. Steps of the proposed wind direction prediction.

Table 1  
Importance of parameters in models (6)–(7) predicting  $s(t)$  and  $c(t)$ .

Parameters of $s(t)$	Importance	Parameters of $c(t)$	Importance
$s(t-1)$	1.000000	$c(t-1)$	1.000000
$s(t-2)$	0.887795	$c(t-2)$	0.899699
$s(t-3)$	0.864507	$c(t-3)$	0.864764
$s(t-4)$	0.862072	$c(t-4)$	0.836095
$s(t-5)$	0.822728	$c(t-5)$	0.823975
$c(t-1)$	0.456624	$s(t-1)$	0.260657
$c(t-2)$	0.259794	$s(t-3)$	0.234974
$c(t-3)$	0.241125	$s(t-2)$	0.200682
$c(t-5)$	0.233592	$s(t-4)$	0.204235
$c(t-4)$	0.222564	$s(t-5)$	0.199367
$w(t-1)$	0.148914	$w(t-2)$	0.169140
$w(t-2)$	0.113982	$w(t-5)$	0.166735
$w(t-3)$	0.098042	$w(t-1)$	0.161363
$w(t-4)$	0.099297	$w(t-3)$	0.136659
$w(t-5)$	0.083507	$w(t-4)$	0.132772

(SVM), neural networks (NN), Random Forest algorithm (RFA) and Gradient Boosted Regression Trees (GBRT), are developed.

SVM is a supervised machine learning algorithm that was initially used in linear classification into two categories. The classification hyper-plane of SVM model is trained based on the

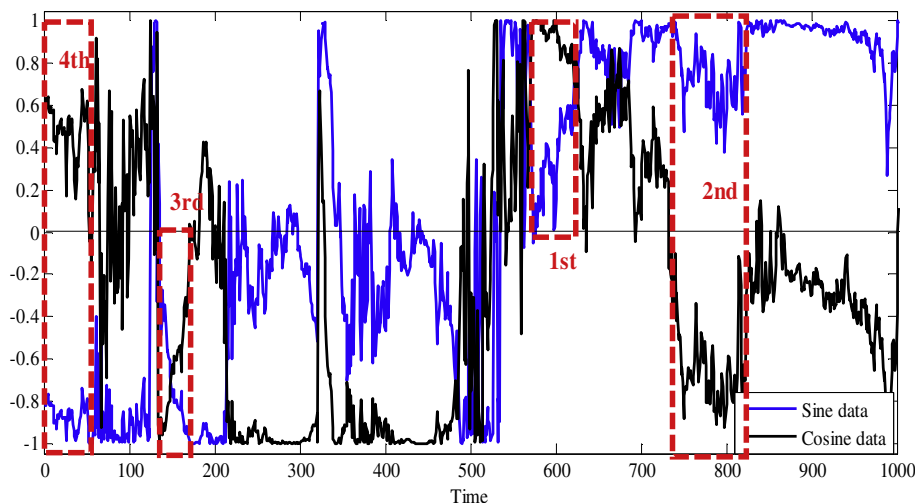


Fig. 7. Values of sine and cosine functions in time.

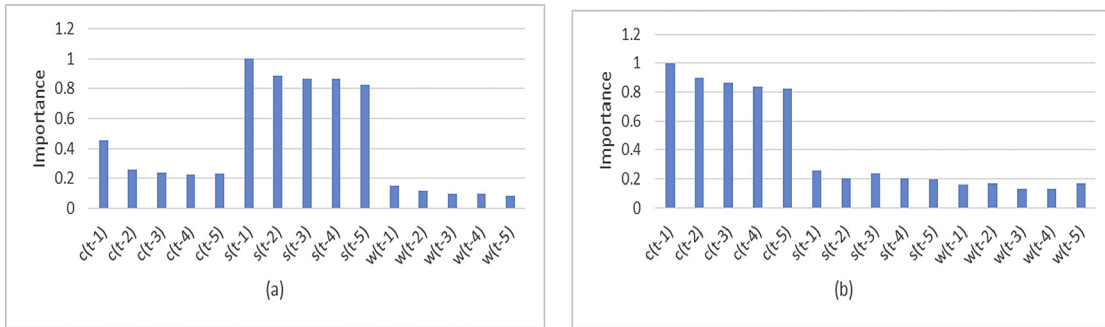


Fig. 9. Bar chart of parameter importance in models (6)–(7): (a) Parameters of  $s(t)$ ; (b) Parameters of  $c(t)$ .

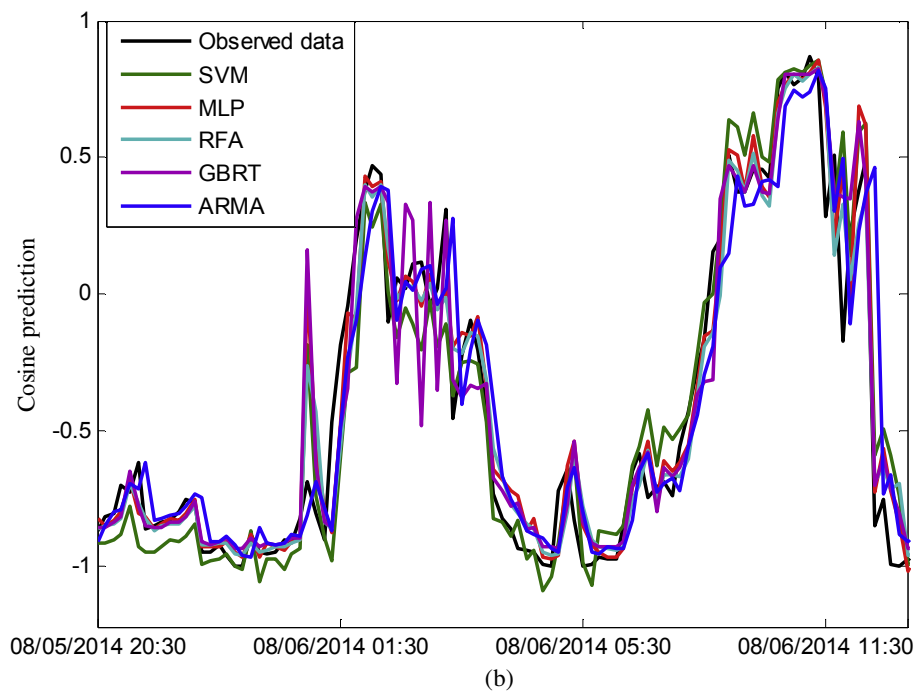
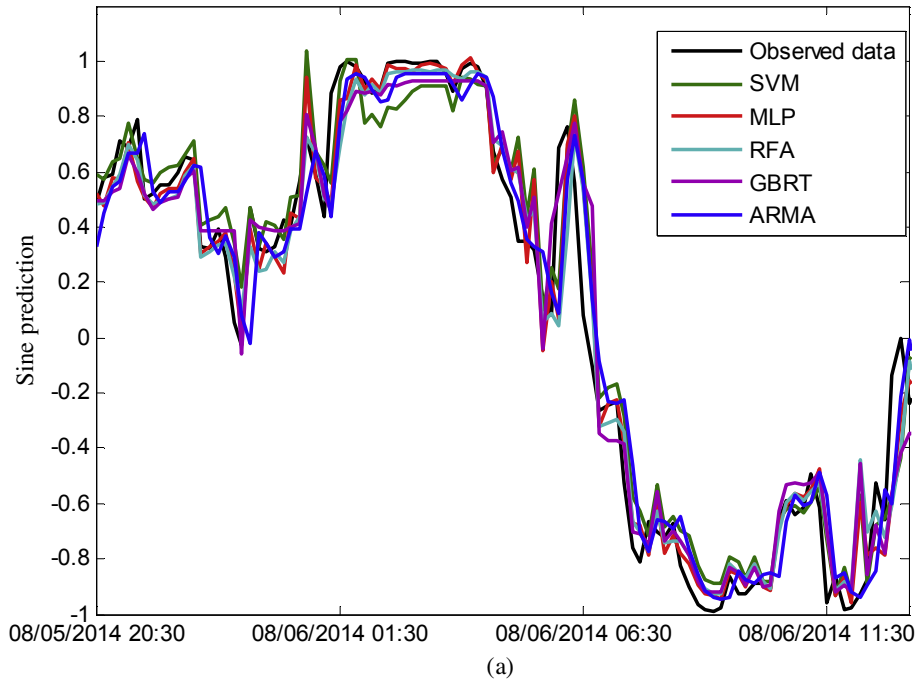


Fig. 10. Prediction of the sine and cosine values with four data mining algorithms: (a) Sine value; (b) Cosine values.

**Table 2**  
Error metrics for the predicted sine values.

	MAE	RMSE	CC
SVM	0.1079	0.1632	0.9719
MLP	0.0935	0.1603	0.9703
RFA	0.0820	0.1468	0.9771
GRBT	0.0993	0.1652	0.9704
ARMA	0.1182	0.2116	0.9511

**Table 3**  
Error metrics for the predicted cosine values.

	MAE	RMSE	CC
SVM	0.1268	0.1815	0.9650
MLP	0.0803	0.1468	0.9766
RFA	0.0869	0.1525	0.9749
GRBT	0.1026	0.1672	0.9701
ARMA	0.1164	0.2027	0.9555

structural risk criterion. SVM was subsequently extended to the support vector regression (SVR). Kernel functions have been introduced to map data points into a high dimension feature space [23].

NN is a computational model inspired by concepts from biology [24]. A NN comprises of interconnected neurons exchanging messages between each other. It has the ability to capture complex relationships between input and output variables. In this paper, a network known as the multilayer perception (MLP) is used.

RFA is an ensemble method used in classification and regression. It includes a multitude of decision trees, the final result is decided by the mean prediction of trees. A collection of decision trees is trained. The bagging technique is used to select the features randomly, and independently sampled data is used for each decision tree [25]. This algorithm is suitable for large data sets, including ones with missing data.

GBRT is a flexible non-parametric learning technique for classification and regression. It combines the advantages of the

regression tree and the gradient boosting algorithm. GBRT is well suited to model complex nonlinear relationships that may include interaction among predictors [26].

### 5. Wind direction prediction and discussion

#### 5.1. Prediction of sine and cosine values

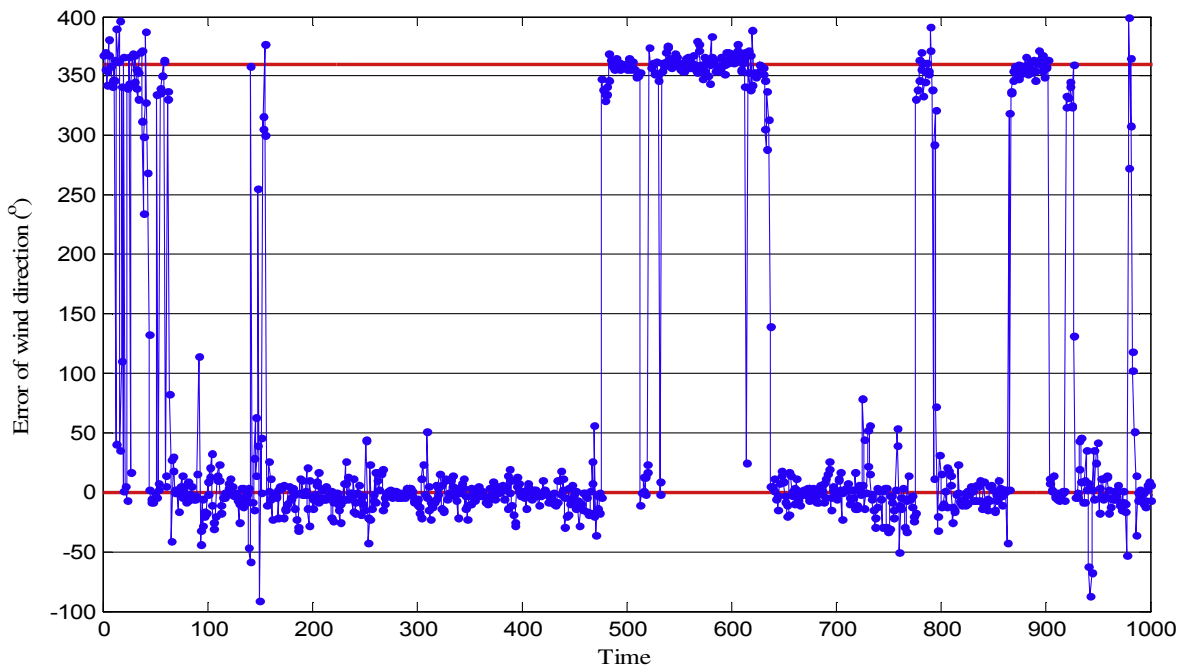
Wind direction data has been transformed into sine and cosine values according to (4). To predict wind direction, four data mining algorithms are utilized to build the prediction model of sine and cosine time series. Fig. 10 illustrates the prediction results.

Fig. 10(a) and (b) shows the prediction results of sine and cosine, respectively. The time period in Fig. 10(a) and (b) is the same, from 08/05/2014 20:30 to 08/06/2014 13:10. The plots in Fig. 10 illustrate different performance of the four models. To assess performance of data mining algorithms, a benchmark model based on ARMA(2,1) was used (see the results in Fig. 10). The best performing model is selected based on the error metrics discussed next.

The errors are classified into longitudinal and transverse errors [27]. The longitudinal errors reflect the long-term performance of system in amplitude measured with the mean absolute error (MAE) and the root mean squared error (RMSE). Transverse errors are applied to performance in time and measured with the correlation coefficient (CC). The three error metrics are defined in (10).

$$\begin{cases} I_{MAE} = \sum_{i=1}^n |x_i - \hat{x}_i| / n \\ I_{RMSE} = \sqrt{\sum_{i=1}^n (x_i - \hat{x}_i)^2 / n} \\ I_{CC} = \frac{\text{cov}(x, \hat{x})}{\sqrt{Dx} \sqrt{D\hat{x}}} \end{cases} \quad (10)$$

where:  $x_i$  is the actual observed points;  $\hat{x}_i$  is the predicted points;  $n$



**Fig. 11.** Absolute error between the predicted and observed wind direction in August 2014.

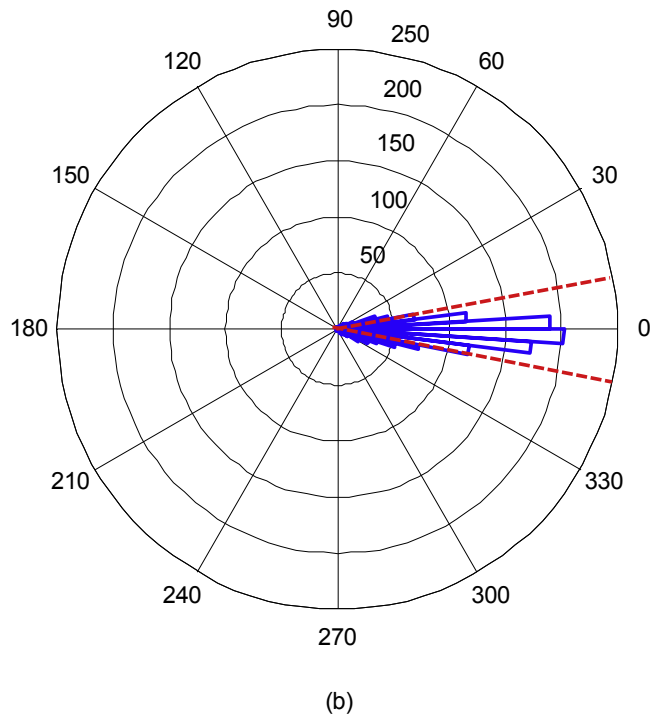
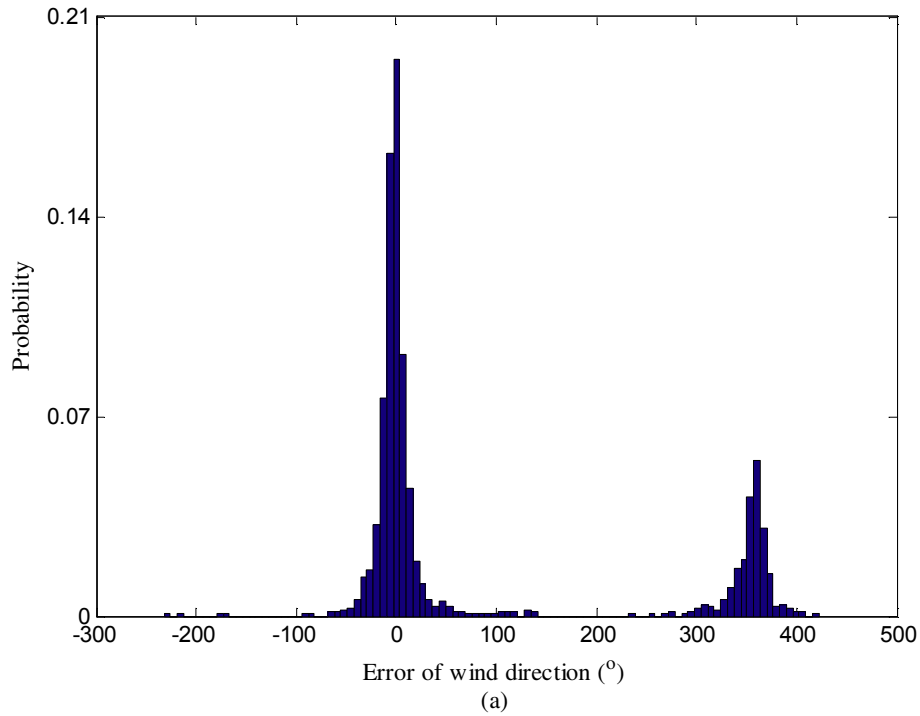


Fig. 12. Distribution of wind direction errors: (a) Histogram; (b) Rose diagram.

is the number of predicted points. Tables 2 and 3 provide values of the three error metrics.

The MAE and RMSE values reflect the amplitude errors and they are expected to be small. A CC value that is close to 1 indicates a good performance of the model. First, the models based on data mining algorithms perform better than ARMA. Second, the random forest algorithm (RFA) performs best in the three error metrics in

Table 4  
Prediction error of the wind direction.

	MAE	RMSE
Traditional method (M1)	9.7737	30.5118
Proposed method (M2)	9.1536	18.7689
Improvement of M2 over M1	6.34%	38.49%

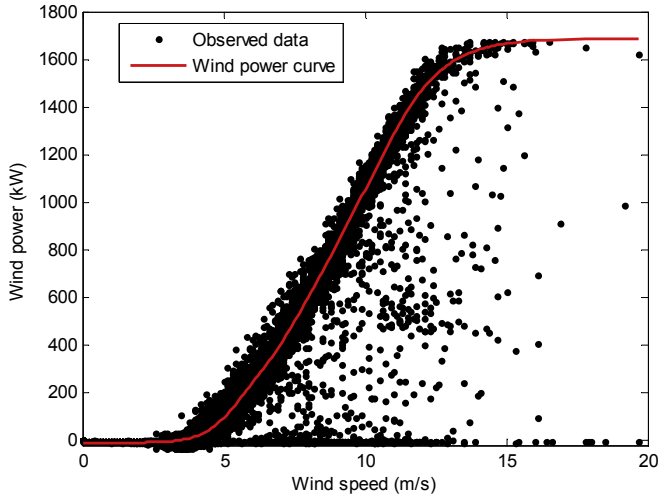


Fig. 13. The wind power curve based on the training data.

Table 5  
Wind power bias computed through wind direction.

	Measured wind direction	Predicted wind direction
Average generation bias	-10.0307	-21.0803
Generation loss	21.4701	19.4450

predicting the sine values in Table 2. The MLP model performs best in predicting the cosine value in Table 3. Therefore, RFA and MLP are selected as the prediction models of sine and cosine value, respectively.

5.2. Error analysis of wind direction

The sine and cosine of the wind direction are predicted by the selected prediction model. The two values are transformed into wind direction. In general, the conversion from the sine/cosine function into an angle presented in (11) is used.

$$\theta = \arctan\left(\frac{\sin(\theta)}{\cos(\theta)}\right) \tag{11}$$

where:  $\theta$  is in the range from  $-90^\circ$  to  $90^\circ$ ,  $\arctan(*)$  is the inverse function of the tangent function. According to Fig. 5, the sign of the tangent function is positive in quadrants 1 and 3 and negative in quadrants 2 and 4. To express the wind direction as a circular variable, the equation is defined in (12) based on (11).

$$D(t) = \arctan\left(\frac{s(t)}{c(t)}\right) + 90^\circ * (1 - \text{sgn}(c(t))) \tag{12}$$

where:  $s(t)$  and  $c(t)$  are the predicted sine and cosine values, respectively,  $\text{sgn}(*)$  is the sign function, and  $D(t)$  is the predicted wind direction. The value of  $180^\circ$  is added to the value  $\theta$  of (11) when the sign of  $c(t)$  is negative, therefore the predicted wind direction  $D(t)$  has a range of  $[-90^\circ, 270^\circ]$ . The predicted sine and cosine values are transformed into wind direction with (12). The

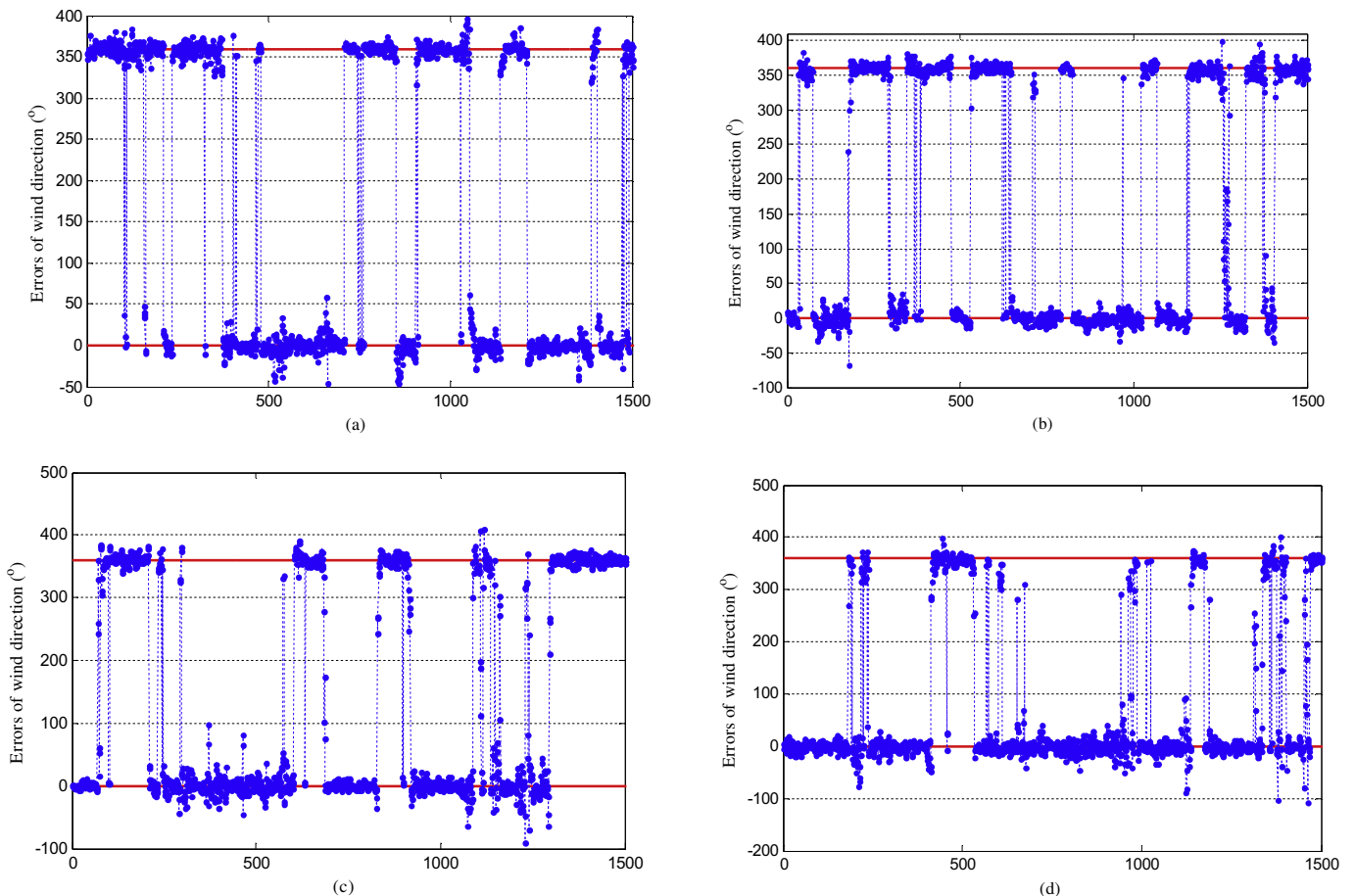


Fig. 14. Absolute prediction errors of the wind direction in the months representing four seasons: (a) October; (b) January; (c) April; (d) June.

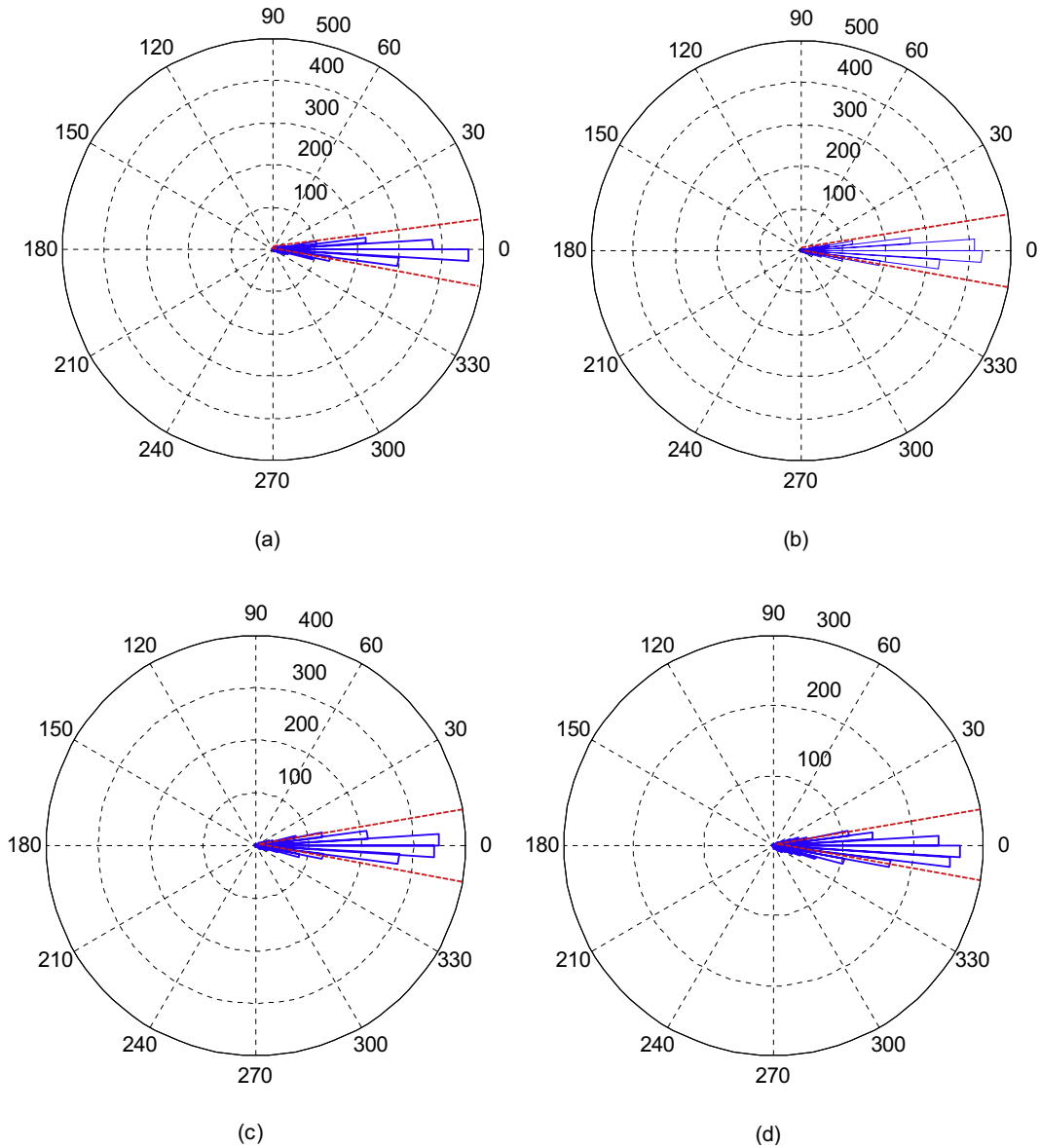


Fig. 15. Rose diagrams of the absolute wind direction errors in the months representing four seasons: (a) October; (b) January; (c) April; (d) June.

absolute error, between the predicted wind direction and the observed data,  $\text{sign} |x_i - \hat{x}_i|$  is shown in Fig. 11.

The horizontal red lines in Fig. 10 represent the angle 0° and 360°, respectively. It can be seen that most absolute error points scatter near these two lines. The prediction errors of the wind direction are illustrated in Fig. 12 as the angle errors.

Fig. 12(a) illustrates the angle distribution of the wind direction error. The angle errors of the predicted wind direction are around 0° and 360°. As wind direction is a circular variable with a period of 360°, 0° and 360° represent the same direction in two dimensional space. Therefore, the rose diagram representation in Fig. 12(b) is considered. Based on the rose diagram, it is reasonable to analyze the angle error of wind direction. The span of the angle errors is less than 720° in Fig. 12(a), the actual angle errors in Fig. 12(b) are adjusted to the span of 0°–360° by (13).

$$e' = e - 180^\circ * (1 - \text{sgn}(180^\circ - e)) \tag{13}$$

where:  $e$  is the angle error,  $e'$  is the adjusted error. The errors

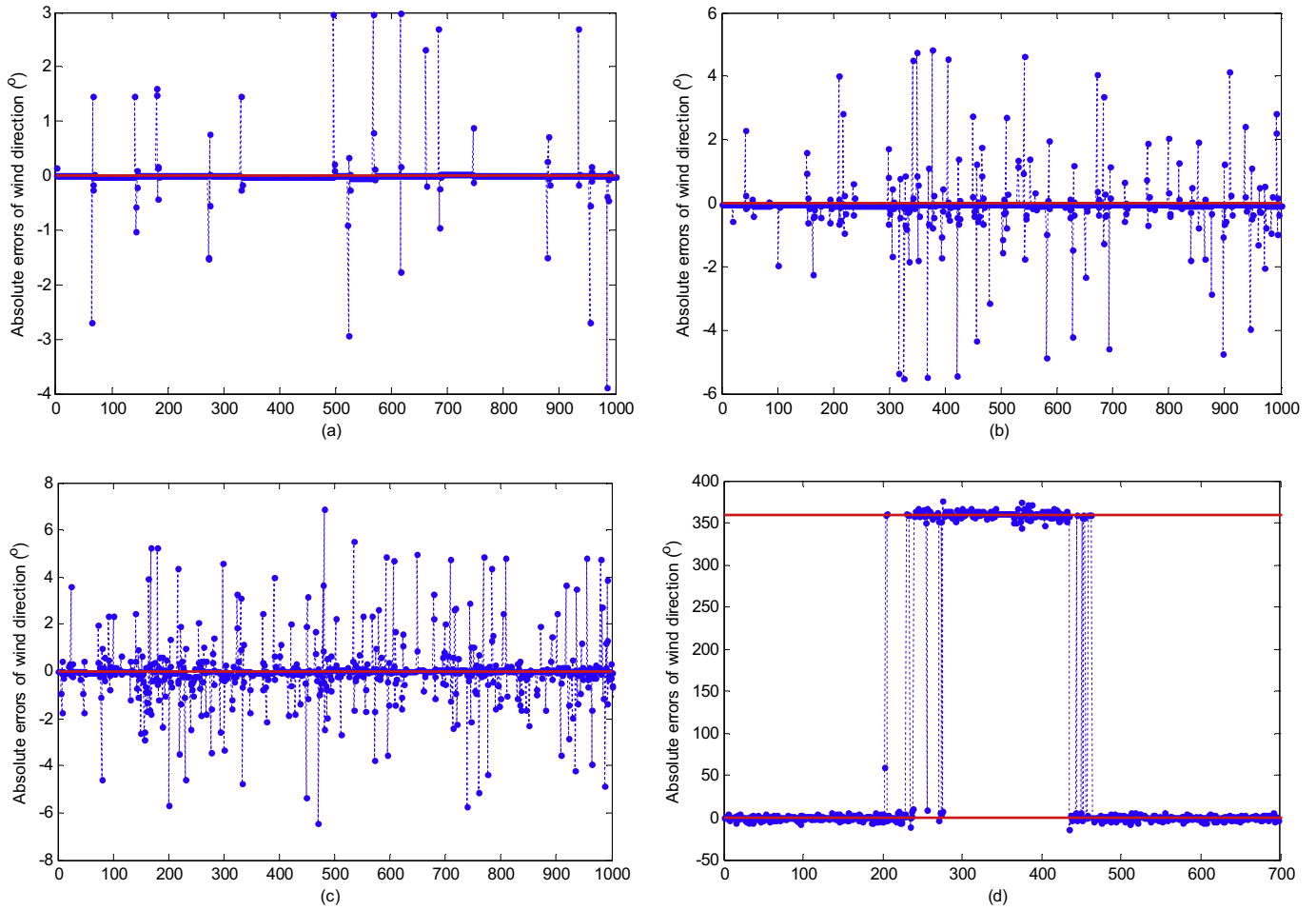
around 360° are adjusted to distribute around 0° through (13), then the error matrixes MAE and RMSE are applicable.

Table 4 illustrates prediction error produced by two wind direction models, M1 and M2, where M1 is the AR(3) model built on the concept of component models [20], M2 represents the proposed model. Performance of the two models M1 and M2 is also compared in Table 4.

Table 4 show the values of MAE and RMSE are smaller for M2 than M1, and the improvement of M2 over M1 is positive implying better performance of model M2. Furthermore, the average prediction error of wind direction is in the interval  $[-10^\circ, 10^\circ]$  (two red lines in Fig. 12(b)) which implies the yaw error is acceptable.

Table 6  
Angle errors at four seasons.

	October	January	April	June
MAE	7.19	7.80	9.57	12.27
RMSE	12.18	14.27	18.15	22.40



**Fig. 16.** Absolute prediction errors of the wind direction with four sampling frequency: (a) Sampling interval of 10sec; (b) Sampling interval of 30sec; (c) Sampling interval of 1min; (d) Sampling interval of 5min.

Yaw error impacts efficiency of power generation. Based on the predicted wind direction, nacelle position, yaw error, and the wind power curve model, the expected wind power is computed. Then expected power and actual power are compared to compute the power loss. The training data is utilized to build a wind power curve in Fig. 13.

Fig. 13 shows the built wind power curve. The solid red line represents the wind power curve built by the data partitioning and mining approach described in Ref. [28]. The expected wind power is computed from the wind power curve model. The power loss is that expected power minus the actual power. For the measured and predicted wind direction, the bias between generated power and the expected power is presented in Table 5.

Table 5 shows the average generation bias and the generation loss for the measured and the predicted wind direction. The average generation bias is computed from all test data. The generation loss is computed by the data points below the wind power curve. The generation bias based on the actual and predicted yaw error is negative, which implies that the generated power is larger than the expected one. The predicted wind direction increases the generated power.

### 5.3. Feasibility analysis

#### 5.3.1. Analysis of data from different seasons

The analysis performed in Section 2 demonstrates that the

prevailing wind direction is seasonal. Four test data sets are selected to validate the proposed model, namely the October, January, April, and June data representing the fall, winter, spring, and summer season, respectively.

Fig. 14(a)–(d) illustrate the prediction results in the month of October, January, April, June, respectively. The results indicate that most error values oscillate around 0° or 360°. Fig. 15 presents distributions of wind direction errors in the form of rose diagrams.

The red broken lines in Fig. 12(a)–(d) represent the angle range of [−10°, 10°]. This indicates that most prediction errors are confined to a small region.

Similarly, Table 6 shows the error matrixes of adjusted angle errors as in Fig. 12. The results confirm high accuracy of the proposed prediction model.

#### 5.3.2. Analysis of different frequency data

To provide more insights into prediction accuracy, the four data-mining algorithms are applied to predict wind direction using higher frequency data. The data with a sampling interval of 10 s,

**Table 7**  
Angle error for four sampling frequencies.

	10 s	30 s	1 min	5 min
MAE	0.08	0.42	0.67	2.26
RMSE	0.38	1.57	1.63	3.94

30 s, 1 min, and 5 min is considered.

Fig. 16(a)–(d) illustrate the prediction results with different sampling frequency. Each model makes one-step-ahead prediction, i.e., 10 s, 30 s, 1 min, and 5 min respectively. In total 1000 points are presented. The results also illustrate that the error values are around 0° or 360°.

Table 7 presents the error produced by the algorithm used to derive data in Tables 2 and 3 for the data sampled at four frequencies. The value of the wind direction predicted at different frequencies (horizons) can be fused for optimal control of the yaw error.

## 6. Conclusion

A data-driven approach to minimize yaw error was presented. This error reduction was accomplished with a model predicting wind direction. The circular variable (wind direction) is transformed into two continuous variables with sine and cosine functions. Four data mining algorithms were used to construct prediction models. Two algorithms, the random forest algorithm and the multilayer perception, were selected to predict the sine and cosine time series. The prediction errors of the wind direction and the sine and cosine values were analyzed across four seasons and four different sampling frequencies. Industrial data was used in model development and error analysis. Computational results have demonstrated high accuracy of the prediction models.

## References

- [1] Bhaskar K, Singh SN. AWNN-assisted wind power forecasting using feed-forward neural network. *IEEE Trans Sustain Energy* 2012;3(2):306–15.
- [2] Global wind energy outlook report. 2010 [online]. Available: <http://www.gwec.net/fileadmin/documents/Publications/GWEO%202010%20final.pdf>.
- [3] Hirata Y, Mandic DP, Suzuki H, Aihara K. Wind direction modelling using multiple observation points. *Philos. Trans R Soc Lond A Math Phys Eng Sci* 1865;2008(366):591–607.
- [4] Monteiro C, Bessa R, Miranda V, Botterud A, Wang J, Conzelmann G. Wind power forecasting: state-of-the-art 2009. Argonne, IL: Argonne National Laboratory; 2009. ANL/DIS-10-1.
- [5] Giebel G, Brownsword R, Kariniotakis G, Denhard M, Draxl C. The state-of-the-art in short-term prediction of wind power: a literature overview. 2011. ANEMOS. plus.
- [6] Kusiak A, Zhang Z, Verma A. Prediction, operations, and condition monitoring in wind energy. *Energy* 2013;60:1–12.
- [7] Gong L, Shi J. On comparing three artificial neural networks for wind speed forecasting. *Appl Energy* 2010;87(23):13–20.
- [8] Kavousi-Fard A, Khosravi A, Nahavandi S. A new fuzzy-based combined prediction interval for wind power forecasting. *IEEE Trans Power Syst* 2016;31(1):18–26.
- [9] Liu Y, Shi J, Yang Y, Lee WJ. Short-term wind-power prediction based on wavelet transform-support vector machine and statistic-characteristics analysis. *IEEE Trans Industry Appl* 2012;48(4):1136–41.
- [10] Liu H, Tian H, Li Y. Comparison of two new ARIMA-ANN and ARIMA-Kalman hybrid methods for wind speed prediction. *Appl Energy* 2012;98:415–24.
- [11] El-Fouly TH, El-Saadany EF, Salama M. One day ahead prediction of wind speed and direction. *IEEE Trans Energy Convers* 2008;23(1):191–201.
- [12] Yang M, Fan S, Lee WJ. Probabilistic short-term wind power forecast using componential sparse Bayesian learning. *IEEE Trans Industry Appl* 2013;49(6):2783–92.
- [13] Bao L, Gneiting T, Gritter EP, Guttorp P, Raftery AE. Bias correction and Bayesian model averaging for ensemble forecasts of surface wind direction. *Mon Weather Rev* 2010;138(5):1811–21.
- [14] Erdem E, Shi J. ARMA based approaches for forecasting the tuple of wind speed and direction. *Appl Energy* 2011;88(4):1405–14.
- [15] Kalusner Z, Kaplan H, Fattal E. The similar day's method for predicting near surface wind vectors. *Meteorol Appl* 2009;16(4):569–79.
- [16] Saleh AE, Moustafa MS, Abo-Al-Ez KM, Abdullah AA. A hybrid neuro-fuzzy power prediction system for wind energy generation. *Int J Electr Power & Energy Syst* 2016;74:384–95.
- [17] Daniele P, Lirer L, Petrosino P, Spinelli N, Peterson R. Applications of the PUFF Model to forecasts of volcanic clouds dispersal from Etna and Vesuvio. *Comput Geosci* 2009;35(5):1035–49.
- [18] McMillan N, Bortnick SM, Irwin ME, Berliner LM. A hierarchical Bayesian model to estimate and forecast ozone through space and time. *Atmos Environ* 2005;39(8):1373–82.
- [19] Finzi G, Fronza G, Rinaldi S. Stochastic modelling and forecast of the dosage area product. *Atmos Environ* 1978;12(4):831–8.
- [20] Carta JA, Ramirez P, Bueno C. A joint probability density function of wind speed and direction for wind energy analysis. *Energy Convers Manag* 2008;49(6):1309–20.
- [21] Fisher NI. *Statistical analysis of circular data*. Cambridge, UK: Cambridge University Press; 1993.
- [22] Kusiak A, Zhang Z. Short-horizon prediction of wind power: a data-driven approach. *IEEE Trans Energy Convers* 2010;25(4):1112–22.
- [23] Wang J, Li L, Niu D, Tan Z. An annual load forecasting model based on support vector regression with differential evolution algorithm. *Appl Energy* 2012;94:65–70.
- [24] Zadpoor AA, Campoli G, Weinans H. Neural network prediction of load from the morphology of trabecular bone. *Appl Math Model* 2013;37(7):5260–76.
- [25] Lahouar A, Slama JBH. Day-ahead load forecast using random forest and expert input selection. *Energy Convers Manag* 2015;103:1040–51.
- [26] Elith J, Leathwick JR, Hastie T. A working guide to boosted regression trees. *J Animal Ecol* 2008;77(4):802–13.
- [27] Lowery C, O'Malley M. Impact of wind forecast error statistics upon unit commitment. *IEEE Trans Sustain Energy* 2012;3(4):760–8.
- [28] Ouyang T, Kusiak A, He Y. Modeling wind-turbine power curve: a data partitioning and mining approach. *Renew Energy* 2017;102:1–8.